Journal of The Electrochemical Society, 2020 **167** 044503

Establishing Performance Baselines for the Oxygen Evolution Reaction in Alkaline Electrolytes

Grace C. Anderson, Bryan S. Pivovar,* and Shaun M. Alia*,z

Chemistry and Nanoscience Center, National Renewable Energy Laboratory, Golden, Colorado 80401, United States of America

This paper establishes baseline performance of several platinum group metal (PGM) and non-PGM catalysts in alkaline oxygen evolution (OER). As OER catalyst development efforts increase, there is a need to standardize testing and baseline performance to compare catalysts between different studies, better direct materials development, and understand how performance improvements translate to the device. Of the catalysts tested, metals tend to have higher half-cell activity than their fully oxidized counterparts. In single-cells, however, metal activities approach oxides, likely due to the elevated temperature, higher potential, and longer time needed to condition membrane electrode assemblies (MEAs) relative to rotating disk electrodes (RDEs). In RDEs, cobalt (Co) and ruthenium nanoparticles are the most OER active. Due to high ruthenium dissolution rates, however, iridium (Ir) is used as a PGM baseline. Activity differences between materials in RDE (Ir 320 A g^{-1}, Co 12 A g^{-1} at 1.55 V) further appear to translate to MEAs (Ir 1370 A g^{-1}, Co 101 A g^{-1} at 1.5 V), indicating that half-cell testing can be useful in the early stages of catalyst development to predict kinetics at the device-level.

 [DOI: 10.1149/1945-7111/ab7090]

Manuscript submitted September 10, 2019; revised manuscript received January 22, 2020. Published February 11, 2020.

Hydrogen is an emerging energy commodity that has many diverse applications and can be integral to achieving energy security. Currently, hydrogen in the United States is mainly used in oil refining and producing ammonia, but can grow to include: storing hydrogen to expand the use of renewable energy sources in the grid; and offloading hydrogen to other sectors such as transportation, agriculture, metal refining, and fuel/chemical synthesis. The predominant method to produce hydrogen is steam methane reforming due to the low cost.[1] While existing commercial electrolysis operations use retail electricity, hydrogen production cost could drop significantly when coupled with intermittent, low-cost renewables.[2] At this point, catalyst development is crucial to reduce capital cost at lower capacity, by using materials that are more active to reduce platinum group metal (PGM) loadings or avoid PGMs altogether. It is similarly important to understand catalyst durability under conditions of low catalyst loading and variable electricity loads.

Compared to proton exchange membrane (PEM) electrolysis, anion exchange membrane (AEM) electrolysis offers several benefits, including the improved stability of metals at high pH and the ability to limit PGM use in the catalyst layers, transport layers, and separators. There has recently been a heightened interest in AEM-based electrolysis due to its potential to reduce hydrogen production cost, and catalyst development in particular due to the potential cost and stability advantages non-PGMs may offer in an alkaline environment. The development of durable catalysts with high activity for OER, particularly non-PGM catalysts, is imperative to reduce the system costs of alkaline water electrolysis and hydrogen production costs overall.

With increasing efforts in OER catalyst development, there is a growing need to establish baseline activities and develop standard test protocols, to improve catalyst comparisons and understand how half-cell performance improvements translate to device level testing. Previous efforts to benchmark alkaline OER catalysts include McCrory et al., which focused on the specific activity of non-PGM oxide films, but did not include evaluation of commercial nanoparticle catalysts to establish baselines.[3] This study seeks to fill this gap through outlining standard testing protocols for AEM half-cell testing and providing baseline catalyst performance in rotating disk electrode (RDE) and membrane electrode assemblies (MEAs). This effort also leverages previous efforts developing standardized test protocols and benchmark performance for OER (PEM electrolysis) and HER (alkaline electrolysis).[4,5]

Experimental

RDE.— *Materials.*—Polished polycrystalline metal electrodes were evaluated for OER activity and used in the calculation of catalyst surface area for RDE tests. The polycrystalline electrodes included nickel (Ni, American Elements, NI-M-03M-D.4MMT), cobalt (Co, American Elements, CO-M-03M-D.4MMT), iridium (Ir, American Elements, IR-M-03M-D.4MMT), ruthenium (Ru, American Elements, RU-M-03M-D.4MMT), and gold (Au, Pine Instrument Co. AFE5T050AU). Prior to use, the polycrystalline electrodes were cleaned in 2-propanol and water and briefly exposed to concentrated nitric, then sulfuric acid. American Elements electrodes (Ni, Co, Ir, Ru) were resurfaced with lapping film (3M) with grades ranging from 30 to 0.3 μm. The resurfaced electrodes were polished with Alumina MicroPolish 0.3 μm (Buehler, 40-6363-006), then 0.05 μm (Buehler, 40-10083) using a MetaServ 250 grinder/polisher (Buehler). Pine Instrument Company electrodes (polycrystalline platinum, Pt and Au), used for reference electrode calibration (Pt) and the working electrode substrate (Au), did not need to be resurfaced but were polished. Prior to RDE testing, all polycrystalline electrodes were cleaned with 2-propanol and water.

The OER activities of various commercial non-PGM and PGM nanoparticle catalysts were evaluated in RDE half-cells. The non-PGM nanoparticle catalysts included Co (Alfa Aesar, 46347), Co_3O_4 (Alfa Aesar, 44661), NiO (Alfa Aesar, 10819), Ni (Alfa Aesar, 45505), Ni (PlasmaChem GmbH), $Fe_{55}Ni_{28}Co_{17}$ (US Research Nanomaterials Inc., US1569), and $NiFe_2O_4$ (US Research Nanomaterials Inc., US3959). The commercial PGM nanoparticle catalysts included Ir (Alfa Aesar, 47150), IrO_2 (Alfa Aesar, 43396), Ru (Premetek, P20V010), Ru (Alfa Aesar, 12354), carbon-supported Ru (40% on Vulcan XC72, Premetek, P20A400), and RuO_2 (Alfa Aesar, 11804). A variety of factors, including morphology (surface area), supports, multicomponents (oxophilicity, alloying), faceting, and oxide content can impact the OER activity of catalysts. No effort was made prior to or during the testing of commercial nanoparticles to modify catalyst surfaces or structure to alter their activity. The intent of this study was to screen commercial materials, as-received, as baseline catalysts in alkaline OER.

*Electrochemical Society Member.
zE-mail: shaun.alia@nrel.gov

RDE testing and catalyst screening.—Each catalyst was tested by depositing an ink onto a Au RDE working electrode with a surface area of 0.196 cm^2. The ink was formulated for a catalyst loading of 17.8 μg_M cm^{-2} and an ionomer mass to catalyst mass ratio of 0.1 μg_{Nafion} $mg_{Catalyst}^{-1}$, previously shown to produce reasonable inks and RDE activities for nanoparticle catalysts intended for PEM fuel cells and electrolyzers.[6] Inks were composed of 3.49 mg catalyst (metal basis) in 7.6 ml of 18.2 mΩ distilled, deionized water (<5 ppb organic carbon content, TOC), 2.4 ml isopropyl alcohol, and 40 μl Nafion ionomer (5 wt%, Sigma-Aldrich, 527084). The catalyst was first added to the water and IPA, iced for five minutes, and then the ionomer was added. The ink was horn sonicated for 30 s, bath sonicated for 20 min, and then horn sonicated for another 30 s. 10 μl of ink was then deposited on the electrode tip rotating at 100 RPM. The speed was then increased to 700 RPM and the electrodes were allowed to dry in air at room temperature.

Half-cell testing was conducted using a three-electrode system in a polytetrafluoroethylene cell (Pine Research Instrumentation, ALK-R-CELL-1). The working electrode rotation speed was controlled by a modulated speed rotator (Pine Research Instrumentation, AFMSRCE), and electrochemical measurements were taken with an Autolab PGSTAT302N potentiostat (Eco Chemie, Metrohm Autolab). The experiments used a catalyst-coated Au working electrode (Pine Research Instrumentation, AFE5T050AU), a Au wire/mesh counter electrode, and a mercury/mercurous oxide reference electrode (Koslow Scientific Company, 5088) connected to the main cell by a handmade Luggin capillary. Electrochemical measurements were taken at room temperature and there was no active temperature control applied to the electrolyte. The laboratory itself (Energy Systems and Integration Facility, Electrochemical Characterization Laboratory at NREL), however, was actively monitored and controlled for temperature at 74.3 °F with a variability of less than 0.1 °F (23.47 °C–23.53 °C) when the experiments were completed.

RDE tests were conducted in a nitrogen saturated 0.1 M NaOH electrolyte (TraceSELECT, Sigma-Aldrich). Prior to testing for OER activity, the reference electrode was calibrated by cycling a polycrystalline Pt electrode in the potential range −0.2–1 V vs RHE (2500 rpm, 10 cycles at 20 mV s^{-1}, potentials approximated from the last calibration) and completing a cathodic linear sweep voltammogram (2500 rpm, 10 mV s^{-1}) in the same potential range. The electrode was immediately removed from the electrolyte with potential (−0.2 V vs RHE) still applied. The intersection between hydrogen oxidation and evolution was taken as the reference potential to calibrate for the experiments that immediately followed. Calibrations were completed following every electrolyte change and a fresh electrolyte was used for each electrode tested.

Additional experiments were completed to minimize contaminant contributions, particularly iron (Fe), through electroplating and chemical processing.[7,8] For electroplating, −0.5 V vs RHE was applied to the polycrystalline Pt electrode for 30 min (following reference electrode calibration) to electroplate metal impurities onto the working electrode; the working electrode was immediately removed with potential still applied. OER measurements on Ir, Ir oxide, Co, Co oxide, Ni, and Ni oxide were repeated and included, with minimal difference found between the calibrated and cleaned (electroplating) electrolytes. Fe removal through chemical processing was also used by previously published methods, where high-purity Ni hydroxide was used to remove Fe in potassium hydroxide electrolytes.[8] This method, however, produced similar activities for the non-PGMs and lower activities for the PGMs, likely due to electrolyte carbonation over time (hours exposed to air, confirmed with a pH decrease from 13 to 10–11), and may be more reflective of the ability of non-PGMs to handle electrolyte deterioration than Fe impurities improving PGM performance. Additional efforts were made to mitigate electrolyte carbonation (nitrogen purge during chemical processing), which lessened the pH and OER activity drop; these results were included, with minimal difference found between the calibrated and cleaned (chemical processing) electrolytes.

Inductively coupled plasma mass spectrometry (ICP-MS) was completed with a ThermoScietific iCAP Q with a dwell time of 0.5 s and run three times per sample with a deviation of less than 2%. The ICP-MS was calibrated to a blank, internal standards, and three standards of known concentration (2, 20, 200 ppb) for the elements of interest (Ni, Co, Ru, Ir, Fe), and potential contaminants (Au from the working electrode, Fe). For Fe, the ICP-MS detection limit (IDL) was 5–10 ppt. For the TraceSelect sodium hydroxide electrolyte (0.1 M), the Fe concentration was 15 ± 3 ppt as prepared and within the detection limit following reference electrode calibration, electrochemical cleaning (electroplating), and chemical processing (Ni hydroxide exposure). Factors may mitigate Fe contamination. The reference electrode calibration may effectively electroplate and remove contaminants; the low Fe concentration in the TraceSelect sodium hydroxide may minimize the issue by providing a start point orders of magnitude less than Fe contaminant effect studies, and ease further removal efforts.[7,8]

Additional considerations were made during RDE testing. Fresh electrolytes were used following each electrode, and the reference electrode recalibrate each time. The PGM catalysts were tested after the non-PGM catalysts to ensure that there was no contamination of the non-PGM catalysts with PGMs (persisted in cell body). The polytetrafluoroethylene cell was periodically cleaned by boiling 8 times in distilled, deionized water; the Au counter was periodically cleaned by soaking in aqua regia, then boiling 8 times in distilled, deionized water.

Half-cell testing of nanoparticle catalysts consisted of electrochemical conditioning (50 cycles, 1.4–1.8 V vs RHE at 50 mV s^{-1} and 2500 rpm), polarization curves (anodic, 1.4–2.0 V vs RHE at 20 mV s^{-1} and 2500 rpm), cyclic voltammetry (0.025–1.6 V at 20, 50, and 100 mV s^{-1}, no rotation), and surface area measurements (depending on the catalyst). Each screened catalyst was held at 1.6 V vs RHE for 13.5 h, previously shown to result in durability losses that reasonably correlated to extended MEA operation in PEM electrolysis.[9] Linear sweep polarization curves, cyclic voltammetry, and surface area measurements were taken of each catalyst following the potential hold. Additional durability testing was completed on Ir and Co nanoparticles, using optimized inks developed in the section below. Experiments were 13.5 h in duration and consisted of: potential holds at 1.4, 1.5, 1.6, 1.8, and 2 V vs RHE for Ir nanoparticles; potential cycles (30,000) between 1.4 V and an upper potential of 1.5, 1.6, 1.8, and 2 V vs RHE for Ir nanoparticles; potential holds at 1.6, 1.8, 2, 2.2, and 2.5 V vs RHE for Co nanoparticles; and potential cycles (30,000) between 1.4 V and an upper potential of 1.6, 1.8, 2, 2.2, and 2.5 V vs RHE for Co nanoparticles. In all durability testing, electrodes were cycled at 2500 rpm to improve transport and bubble detachment. OER mass activity following durability testing was calculated based on the observed current in the kinetic region and the initial catalyst mass coated on the working electrode.

Ink optimization.—For the PGM and non-PGM catalysts screened, Ir and Co nanoparticles were further optimized and evaluated as baselines since: the Co nanoparticles were the highest performing non-PGM catalyst; and the Ir nanoparticles had a significantly lower dissolution rate than Ru. Ink optimization for these catalysts consisted of varying catalyst loading and ionomer content. Catalyst loadings of 8.9, 17.8, 35.6, and 71.2 μg_M cm^{-2} and ionomer contents of 0, 5.71, 11.43, 45.71, and 91.43 μl $mg^{-1}{}_M$ were used, and optimum inks were determined from mass activity. The optimum Ir ink resulted in a loading of 17.8 μg_M cm^{-2} and ionomer content of 0.1 μg_{Nafion} $mg^{-1}{}_M$. The optimum Co ink resulted in a loading of 71.2 μg_M cm^{-2} and ionomer content of 0.1 μg_{Nafion} $mg^{-1}{}_M$. These inks were used to coat electrodes for durability testing (potential holds, cycles) discussed in the above section. For Ir, the OER mass activity declined at higher loading, likely due to lower utilization with thicker catalyst layers. For Co, however, the mass activity was relatively constant up to 71.2 μg_M cm^{-2}, which may have been due to the larger particle size (30 nm Co, 5 nm Ir). The

higher catalyst loading was used to provide a larger current density in the kinetic region (accuracy) and a current density comparable to Ir to ensure that durability comparisons were not impacted by the gas generation rate. Similar activity losses and dissolution rates were found for Co nanoparticles at a lower catalyst loading (17.8 μg_M cm^{-2}). Optimized electrodes contained 0.1 μg_{Nafion} $mg^{-1}{}_M$: at lower ionomer content the activity dropped, likely due to poorly dispersed inks; at higher ionomer content the activity dropped, likely due to contaminant effects. These results (0.1 μg_{Nafion} $mg^{-1}{}_M$ optimum) and trends are similar to those previously observed in alkaline hydrogen evolution and acidic OER.[4,5]

Surface area calculation.—Catalyst surface areas were determined through a combination of carbon monoxide oxidation, hydrogen underpotential deposition, metal redox, and capacitance. For Ir and Ru, surface areas were determined by carbon monoxide oxidation. Electrodes were held at 0.2 V for 20 min, the first 10 min with carbon monoxide and the second 10 min with nitrogen saturating the electrolyte. Following the 20 min hold, the electrodes were cycled in the potential range 0.025–1.0 V vs RHE and at a scan rate of 20 mV s^{-1}. The first cycle was used to calculate surface area and the following cycles to ensure that excess carbon monoxide was removed during the nitrogen purge. Electrochemical surface areas were calculated assuming a Coulombic charge of 358 μC cm^{-2} (carbon monoxide oxidation for Ir, Ru).[10] Ru and Ir surface areas were confirmed with hydrogen underpotential deposition, from the charge due to an adsorbed monolayer during cycling voltammograms in the potential range 0.025–1.0 V vs RHE and at a scan rate of 20 mV s^{-1}, assuming a Coulombic charge of 179 μC cm^{-2} (hydrogen underpotential deposition for Ir, Ru).[10] For Ir and Ru oxide, the surface area was approximated from the capacitance during cycling voltammograms in the potential range 0–1.5 V vs RHE and by varying the scan rate (10, 20, 50, and 100 mV s^{-1}). The double layer charging current was equal to the scan rate multiplied by the electrochemical double-layer capacitance.[3] Surface areas were calculated with a double-layer capacitance of 589 μF cm^{-2} (capacitance for Ir oxide, Ru oxide), previously determined from the linear relationship between the double-layer current and scan rate (slope of 0.59 mF), and the electrochemical surface area determined by mercury underpotential deposition (28.7 m^2 g^{-1} at 17.8 μg cm^{-2}).[11]

For Co- and Ni-based catalysts, the surface area was approximated from the charge due to surface oxidation during cyclic voltammograms in the potential range 0–1.5 V vs RHE and at a scan rate of 20 mV s^{-1}. Polycrystalline electrodes were used to establish a Coulombic charge conversion and assumed a roughness factor of 1.25, an average of the roughness factors for the PGM polycrystalline electrodes evaluated (Pt 1.29, Au 1.20, Ir 1.27, Ru 1.24). For Co, surface oxidation included a transition from $Co(OH)_2$ to Co_3O_4 and $Co(OH)_3$, and the surface areas were calculated with a charge factor of 3.51 mC $cm_{Co}{}^{-2}$. For Ni, surface oxidation included a transition from $Ni(OH)_2$ to Ni_3O_4, Ni_2O_3, and NiO_2, and the surface areas were calculated with a charge factor of 3.76 mC $cm_{Ni}{}^{-2}$. For Co oxide and Ni oxide based catalysts, surface areas were determined from the charge due to surface oxidation and were confirmed with capacitance.[3,11]

Single-cell flowing electrolyte.—Single-cell testing used Sustainion® membranes and ionomers to evaluate benchmark catalysts. Other ionomers may have different catalyst-ionomer interactions, and the baseline cell performances presented here are limited to this membrane/ionomer combination and with a supporting electrolyte.

Single-cell testing of the commercial Co, Co_3O_4, Ir, and IrO_2 catalysts in a flowing electrolyte system was conducted to provide standardized performance for single-cell electrolysis. Non-PGM catalyst layers (NiFe oxide, and CoFeNi) were obtained from Dioxide Materials and tested to ensure that the MEA performance was consistent with the findings of Liu et al.[12] Once a similar performance was achieved, the commercial nanoparticles (Co, Co_3O_4, Ir, and IrO_2) were tested as baseline materials to avoid advanced and optimized catalysts. All plots were corrected for the high frequency resistance unless specified otherwise. The tests used Pt/HSC cathodes with a loading of 0.1 mg cm^{-2} to ensure that measured performance changes were based on the OER catalyst. Non-PGM catalysts Co and Co_3O_4 at the anode were tested with loadings of 0.45 mg cm^{-2}, and IrO_2 and Ir were tested with loadings of 0.1 mg cm^{-2}. Loadings were confirmed with X-ray fluorescence (XRF), with measurements taken 4 times at 30 s exposures on a XDV-SDD.

The catalysts were coated onto 5% PTFE Toray carbon paper to produce gas diffusion electrodes (GDEs) used as anodes in the cell. Inks were created with 52.5 mg metal catalyst, 1.2 ml 18 mΩ deionized water and 10.8 ml IPA. The ink was iced for five minutes, then 48.6 mg of Sustanion® XB-7 ionomer (5% in ethanol) was added. The ink was horn sonicated for 30 s, bath sonicated for 20 min, and horn sonicated for another 30 s. The inks were sprayed with an approximate loading of 0.45 mg cm^{-2} verified with XRF. In MEA testing, Pt/HSC (47% Pt, Tanaka Kikinzoku Kogyo, TEC10E50E) was used at the cathode, sprayed on Toray GDEs with a loading of 0.1 mg_{Pt} cm^{-2}. All single-cell testing was done in 1 M KOH and 0.1 potassium bicarbonate using Sustainion® Alkaline Anion Exchange Membrane X37-50 grade T.

The single-cell tests used Fuel Cell Technology aluminum end plates, Au current collectors, and Ni triple-serpentine flow fields, with Ni tubing to prevent electrolyte contact with aluminum. The cell was controlled with an Autolab PGSTAT302N potentiostat (Eco Chemie, Metrohm Autolab) and a 20 A Autolab Booster (Eco Chemie, Metrohm Autolab). MEAs were conditioned with a 2 V potential hold, followed by polarization curves from 1.4 V to 2 V, cyclic voltammetry, and electrochemical impedance measurements. These procedures were completed at 60 °C and repeated at 80 °C.

Results and Discussion

Polycrystalline electrodes.—Polycrystalline Ir, Ru, Co, and Ni electrodes were evaluated for OER activity, in order to: verify general activity trends; assess differences in activity between polycrystalline electrodes and their nanoparticle counterparts; and determine electrochemical surface areas for evaluating the specific activities of commercial nanoparticles (Figs. 1a and 1b). The observed current densities were kinetic below 0.1 A $cm_{elec}{}^{-2}$; deviations from Tafel slopes at higher current density were reflective of increasing transport loss. Compared to the baselining results by McCrory et al., the overpotentials in this study followed a similar pattern (Ru < Ir < Co/Ni), with the exception that Ni had slightly higher kinetic activity than Co.[3] Compared to the commercial nanoparticles, Ru, Ni, and Co polycrystalline electrodes had lower potentials and higher specific activities than their metal nanoparticle catalysts. For Ru in particular, a large gap was observed, which may be reflective of Ru nanoparticle dissolution during electrochemical conditioning. Higher polycrystalline performance (Ru, Co, Ni) may also be due to the extended surface which can avoid less active, fringe facets, and low coordination number sites. Polycrystalline electrodes were used to establish Coulombic charge conversions for nanoparticle-based catalysts, in order to determine electrochemical surface areas and site-specific activities. For PGM catalysts that were primarily metallic ex situ, electrochemical surface areas were determined from carbon monoxide oxidation and verified with hydrogen underpotential deposition. PGM oxide surface areas were approximated from capacitance using previously established methods.[3,11] Co and Ni metal surface areas were determined for the charge associated with the oxidation of $Co(OH)_2$ to $Co(OH)_3$ and $Ni(OH)_2$ to NiO_2, respectively. These calculations used Coulombic charge conversions of 3.51 mC $cm_{Co}{}^{-2}$ and 3.76 mC $cm_{Ni}{}^{-2}$ assuming a roughness factor of 1.25, an average of the roughness factors for the PGMs (Pt 1.29, Au 1.20, Ir 1.27, Ru 1.24).

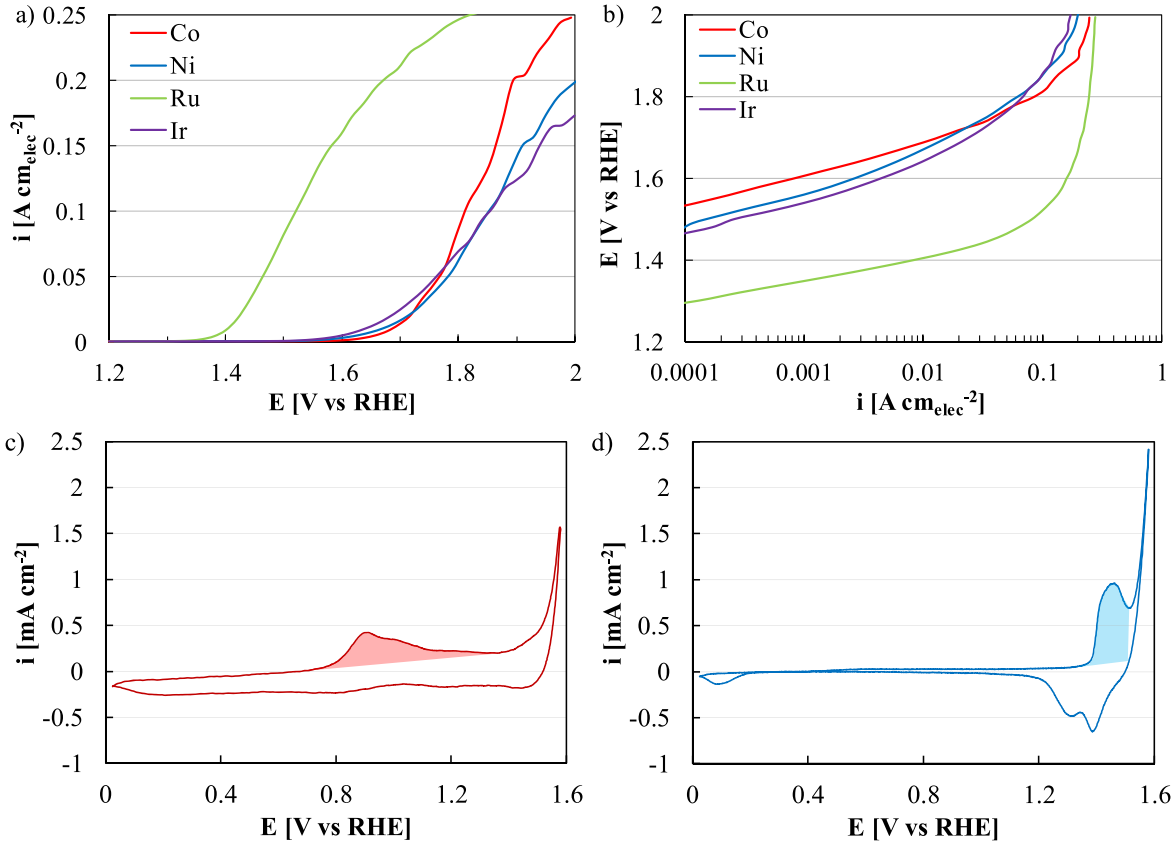

Figure 1. Activity of polycrystalline Co, Ir, Ni, and Ru electrodes in RDE, presented as (a) full linear sweep voltammograms and (b) with a focus on the kinetic region. Cyclic voltammograms of polycrystalline (c) Co and (d) Ni electrodes, used to calculate electrochemical surface areas. The integrated areas accounting for $Co(OH)_2$ oxidation to $Co(OH)_3$ (red) and Ni_3O_4 oxidation to NiO_2 (blue) were highlighted.

Commercial nanoparticles.—Commercial nanoparticles were screened in this study, including Co- and Ni-based catalysts as non-PGMs and Ir- and Ru-based catalysts as PGMs, since they have previously been shown to be active for OER.[13] Of the non-PGM catalysts tested, Co (metal) had the highest OER activity and lowest overpotential, followed by Ni (PlasmaChem, GmbH) and $NiFe_2O_4$ (Figs. 2a and 2b). In general, the catalysts that began as primarily metallic ex situ tended to have higher OER activity than the oxides, consistent with previous findings in acidic electrolytes.[14] Similarly, Ir and Ru metal had higher OER activities and lower overpotentials than their oxides (Figs. 2c and 2d). While Ru was expected to have higher OER activity than Ir, significant Ru dissolution may have occurred during electrochemical conditioning and negated a benefit. Carbon supported Ru (40% Vulcan XC-72, Premetek) and unsupported Ru (Alfa Aesar) were also evaluated but not included since the catalysts completely dissolved from the electrode surface during conditioning. While RDE activities could be taken without conditioning or at moderate potential to avoid dissolution and preserve surfaces, conditioning at 1.2–1.8 V vs RHE was used in an effort to relate RDE activity to MEA performance.

To compare the OER activities of PGM and non-PGM catalysts, the kinetic activities were compared at 1.55 V vs RHE (Fig. 3). This potential was used since it was low enough to avoid transport for the PGM catalysts, while high enough to capture kinetics for the majority of non-PGM catalysts (avoid capacitance). The Tafel slope was the lowest for Ir at 49 mV dec^{-1} (PGM) and Co at 68 mV dec^{-1} (non-PGM), the former comparable to previous findings in acidic electrolytes.[4] For the other catalysts, however, the Tafel slopes were higher. These differences highlight the difficulties in making kinetic comparisons between different material types, and comparisons at different potentials or currents would enlarge or reduce performance gaps. Of the catalysts tested, unsupported Ir had the highest mass activity (320 A g_{Ir}^{-1} at 1.55 V) and unsupported Ru (metal) had the highest specific activity (11.6 μA cm_{Ru}^{-2} at 1.55 V). Deviations from kinetics for each catalyst is visible in the Tafel plots due to capacitance at low potential and transport at high potential (Figs. 2b and 2d). Transport, as opposed to internal resistance changes, was confirmed with resistance corrections, activity reproducibility (slow oxide growth), and visually when completed in glass cells. The transport losses were more severe for Co_3O_4, Ni (PlasmaChem GmbH), Ir, and IrO_2, which may reflect differences in surface area, catalyst structure, and how materials handle bubble formation and detachment.

Additional experiments were completed using electroplating and chemical processing to remove electrolyte impurities (Fe). Following electroplating and chemical processing (following nitrogen purge to mitigate carbonation), a significant change in activity was not observed for the catalysts tested, including: Ir and Ir oxide (Fig. 4a); Co and Co oxide (Fig. 4b); and Ni (Alfa Aesar), Ni (PlasmaChem GmbH), and Ni oxide (Fig. 4c) nanoparticles. The absence of an Fe effect may have been due to RDE test protocols, where reference electrode calibration on a polycrystalline Pt electrode may have removed Fe impurities. The TraceSelect sodium hydroxide electrolyte may have also minimized an Fe effect, with an electrolyte-Fe concentration orders of magnitude below typical contaminant observations or the low concentration easing removal efforts.[7,8] For the electrolyte as-prepared, the Fe concentration was 15 ± 3 ppt; following reference electrode calibration and electrochemical cleaning (electroplating, chemical processing), the Fe concentration was within the ICP-MS detection limit (IDL, 5–10 ppt for Fe). Fe contamination did not appear to be a significant issue in these experiments; depending on the electrolyte source and RDE cleaning and testing protocols, however, significant contaminant issues may occur and removal efforts may be necessary.[8]

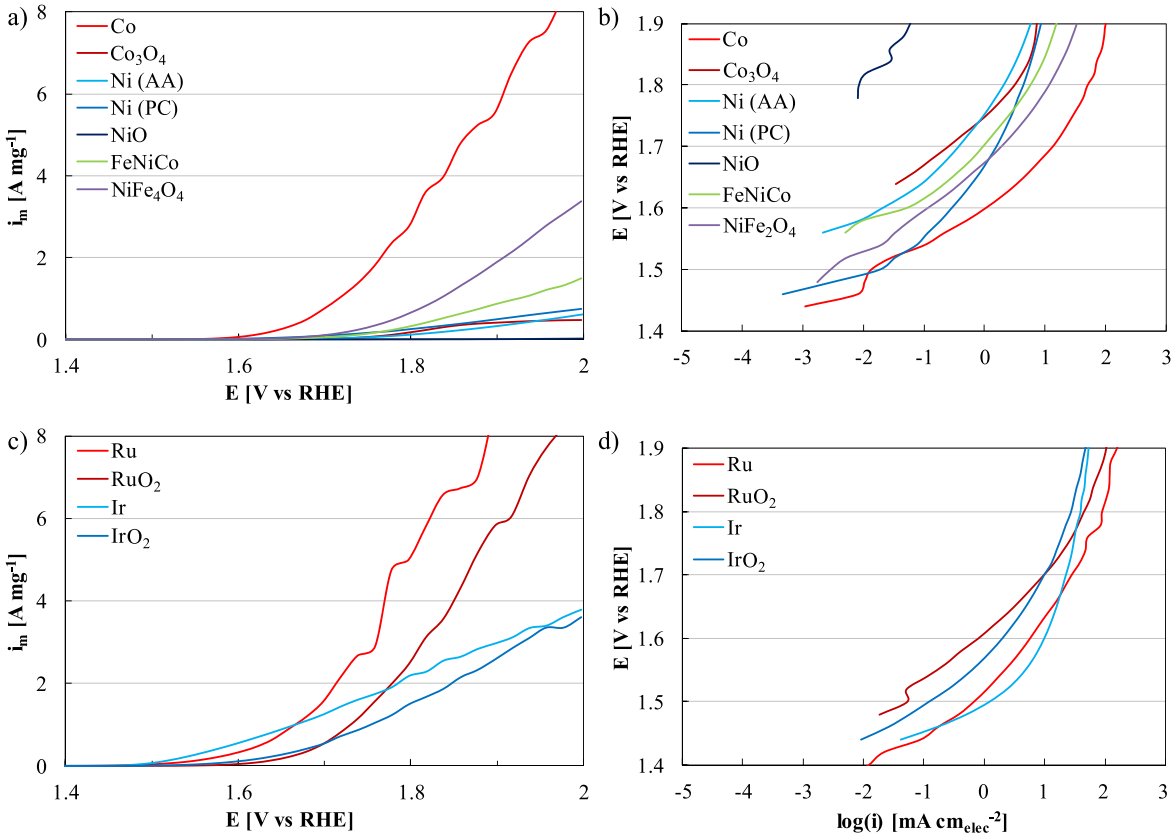

Figure 2. OER mass activity of (a), (b) non-PGM and (c), (d) PGM catalysts, presented as (a), (c) full linear sweep voltammograms and (b), (d) with a focus on kinetics.

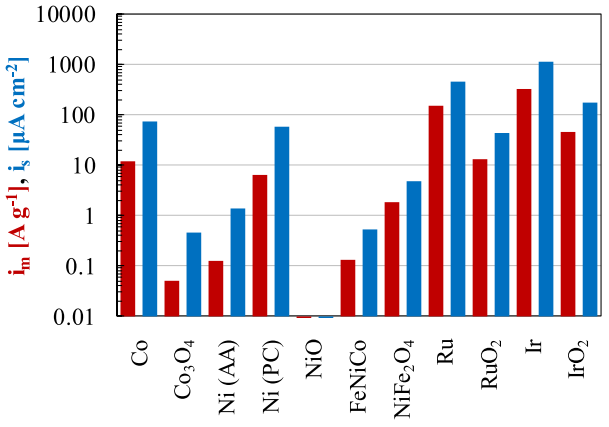

Catalyst	i_m [A g^{-1}]	i_s [μA cm^{-2}]	Tafel Slope [mV dec^{-1}]
Co	12.2	72.7	68
Co_3O_4	0.05	0.5	81
Ni (AA)	0.1	1.4	93
Ni (PC)	6.5	57.2	101
NiO	0.0008	0.003	149
FeNiCo	0.1	0.5	99
$NiFe_2O_4$	1.8	4.8	86
Ru	154.2	465.8	90
RuO_2	12.9	43.3	83
Ir	318.9	1149.6	49
IrO_2	44.6	170.8	106

Figure 3. Mass (red) and specific (blue) activities of non-PGM and PGM catalysts for the OER at 1.55 V vs RHE, presented (a) graphically and (b) in a table with Tafel slopes included.

Benchmarking review.—The catalyst OER performances in this study were compared to published values in literature. This comparison reflects baseline values, not a survey of catalyst development efforts where improvements in OER activity were made through modifications to electrochemical surface areas (morphology, supports) or specific activity (faceting, alloying, multicomponents).[13] Discrepancies between the baseline values in this report and in the literature may be due to a variety of factors such as the catalyst manufacturer, composition, and conditioning procedure. These differences highlight the need for universally applied baselines, as reported baseline catalyst performances can vary by several orders of magnitude.

Many of the studies reviewed used the Nernst equation to convert potentials to the standard hydrogen electrode (SHE) from saturated calomel electrodes,[11,15–46] silver/silver chloride electrodes,[42,47–72] and mercury/mercurous oxide electrodes.[73–82] Other studies have reported catalyst activities at potentials with respect to experimental references (saturated calomel, silver/silver chloride, mercury/mercurous oxide).[83–97] These studies were not included in the OER baseline comparisons due to difficulties translating between the experimental reference, SHE, and RHE values (Tables I, II). The activities in Tables I and II were also reported with respect to potential. On occasion, RDE catalyst performance is reported with respect to the overpotential at 10 mA cm^{-2}, in an effort to translate

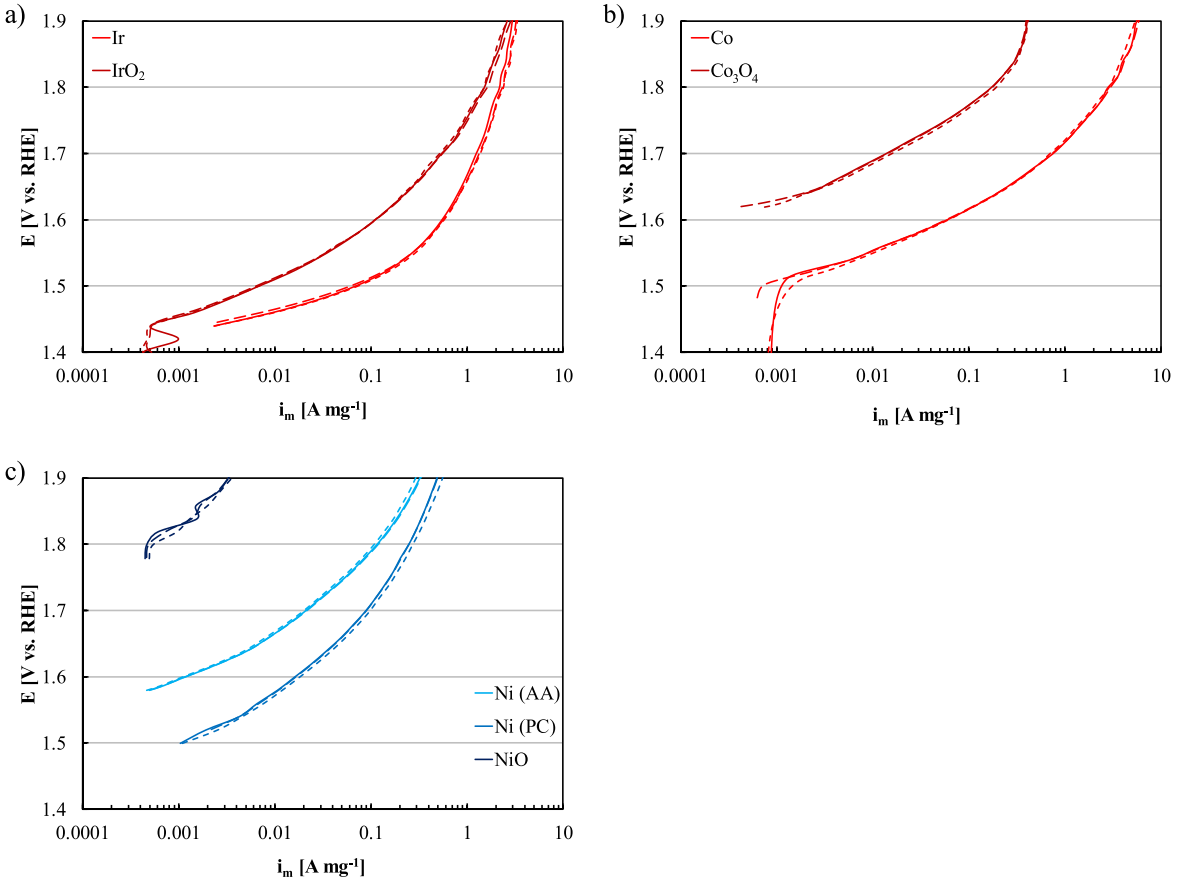

Figure 4. Mass activities of (a) Ir, (b) Co, and (c) Ni-based nanoparticle catalysts following reference electrode calibration (solid line), electrolyte cleaning by electroplating (short-dashed line), and electrolyte cleaning chemical processing (long-dashed line).

RDE activity to MEA performance. While current density-based approaches are useful as qualitative comparisons, this methodology was avoided since it can overstate the role kinetics play in MEAs, where kinetics is not the only or typically the largest source of loss (ohmic) at operating current densities.

RDE durability.—In durability testing, Ir and Co were evaluated since they were representative of materials with higher activities for PGM and non-PGM catalysts. Ru wasn't included due to the high dissolution rate and large losses observed during conditioning.[121] Initial screening for catalyst durability consisted of potential holds at 1.6, 1.8, and 2 V and cycles between 1.4 V and an upper potential of 1.6, 1.8, and 2 V. Additional holds and cycles were completed: to lower potentials (1.4, 1.5 V) on Ir since dissolution occurred at moderate potential; and to higher potentials (2.2, 2.5 V) on Co since minimal dissolution was found. OER mass activities following durability testing were calculated based on the observed current in the kinetic region and the initial catalyst mass coated on the working electrode.

Performance losses were generally similar for potential holds and cycles, expected since the potential range did not cycle through Co or Ir redox.[121] For Ir, losses occurred at moderate potential (73%, 1.4 V hold) with minimal dissolution (Table III, Table IV, Fig. 5a). These losses were likely due to oxide growth, previously found in acidic electrolytes.[14] The activity decrease in base, however, was larger and may be due to the lower specific activity of Ir oxide relative to Ir metal (order of magnitude, Figs. 2d, 3). Larger Ir-activity losses were found when held or cycled to high potential and

Table I. Summary of published baseline OER catalyst mass activities in 0.1 M KOH at 1.55 V vs RHE.

Author	Reference	Catalyst	Details	Metal % [wt%]	i_m 1.55 V [A g^{-1}]
Y. Lee et al.	98	RuO_2	Sigma-Aldrich	—	26
F. Liang et al.	99	RuO_2	3–5 nm	—	6
M. Gao et al.	100	RuO_2	Sigma-Aldrich	—	30.2
Y. Gorlin et al.	101	Ir/Vulcan	Premetek	20	125
M. Gong et al.	102	Ir/Vulcan	Premetek	20	27.5
H. Wang et al.	103	Ir/Vulcan	Premetek	20	48
G. Anderson et al.	—	Ir	Johnson Matthey Corp	—	320
Y. Zhu et al.	104	IrO_2	Aladdin Industrial Corp.	—	11
Y. Zhu et al.	105	IrO_2	Aladdin Co., Ltd.	—	11
T. Maiyalagan et al.	106	IrO_2	Alfa Aesar	—	60
J. Parrondo et al.	107	IrO_2	—	—	12.5
G. Anderson et al.	—	Co	Alfa Aesar	99.8	12

Table II. Summary of published baseline OER catalyst mass activities in 1 M KOH at 1.55 V vs RHE.

Author	Reference	Catalyst	Details	Metal % [wt%]	i_m 1.55 V [A g^{-1}]
Y. Yang et al.	108	RuO_2	—	—	160
B. Zhang et al.	109	RuO_2	Alfa Aesar	—	61
W. Zhu et al.	44	RuO_2/Ni Foam	—	—	1.5
Y. Wu et al.	110	RuO_2	Aladdin	—	5
T. Liu et al.	111	RuO_2/Ti	—	—	20
T. Liu et al.	112	RuO_2/Ti	—	—	7
Y. Wu et al.	110	IrO_2	synthesized	20	9
B. You et al.	113	IrO_2	Alfa Aesar	—	18
L. Trotochaud et al.	114	IrO_2	Stream Chemicals	—	15
J. Wang et al.	115	IrO_2	Johnson Matthey Corp	—	25
X. Cui et al.	116	IrO_2	—	—	69
F. Song et al.	117	IrO_2	—	—	35
J. Vigil et al.	118	Ir/C	—	—	13
X. Liu et al.	119	Ir/C	Vulcan XC-72R	20	5
Y. Jin et al.	120	Pt/C	TKK, Japan	46.7	19

Table III. Mass activity and performance change following durability testing for Co and Ir nanoparticles. Durability tests were completed by potential hold (13.5 h) in a 0.1 M NaOH electrolyte. OER mass activities following durability testing were calculated based on the initial catalyst mass coated on the working electrode.

Potential Hold [V]	Ir Activity Initial [A g^{-1}]	Ir Activity Final [A g^{-1}]	Ir Activity Loss [%]	Co Activity Initial [A g^{-1}]	Co Activity Final [A g^{-1}]	Co Activity Loss [%]
1.4	119	32	73	—	—	—
1.5	155	12	92	—	—	—
1.6	245	50	78	26	7	84
1.8	149	12	92	22	3	88
2	154	2	98	24	3	64

Table IV. Mass activity and performance change following durability testing for Co and Ir nanoparticles. Durability tests were completed by potential cycles (13.5 h) in a 0.1 M NaOH electrolyte. OER mass activities following durability testing were calculated based on the initial catalyst mass coated on the working electrode.

Potential Cycle [V]	Ir Activity Initial [A g^{-1}]	Ir Activity Final [A g^{-1}]	Ir Activity Loss [%]	Co Activity Initial [A g^{-1}]	Co Activity Final [A g^{-1}]	Co Activity Loss [%]
1.4–1.5	115	13	88	—	—	—
1.4–1.6	180	41	77	28	4	72
1.4–1.8	161	12	93	22	3	86
1.4–2	143	8	95	27	9	81

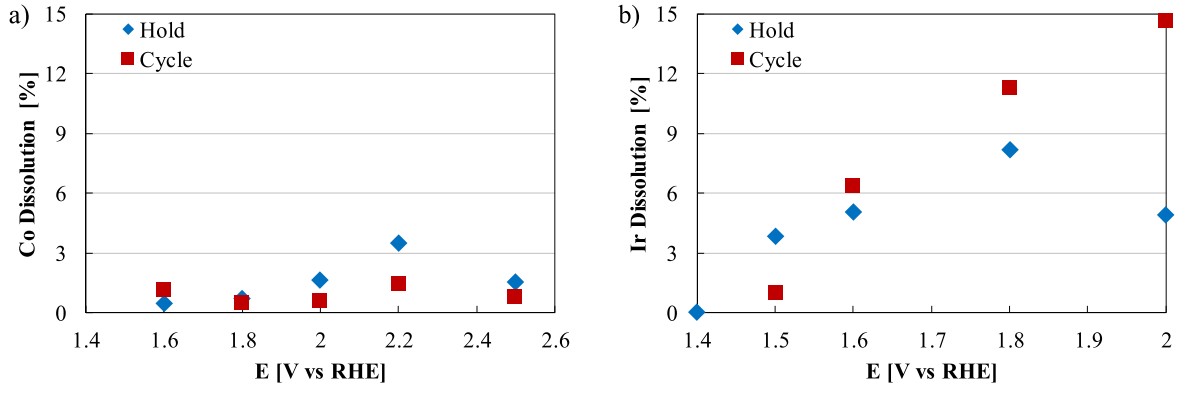

Figure 5. Dissolution of (a) Co and (b) Ir nanoparticles in durability testing by potential cycles (red) and holds (blue), determined by ICP-MS.

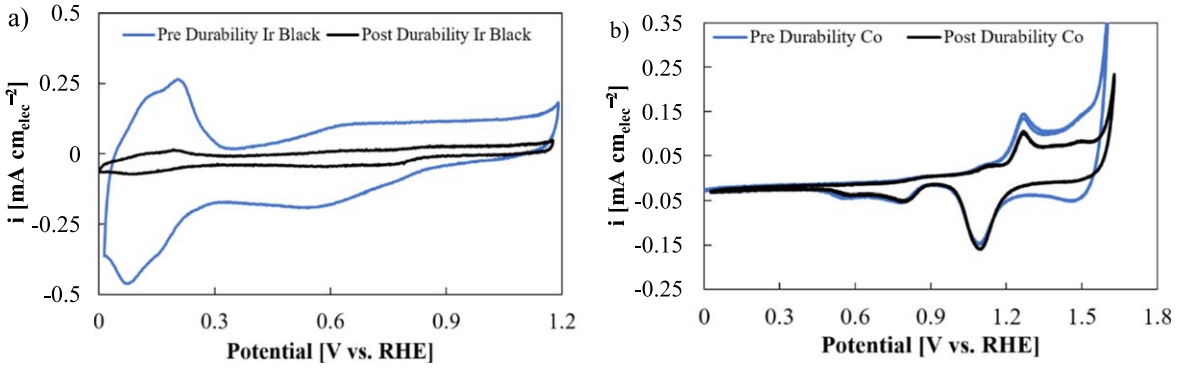

Figure 6. Cyclic voltammograms (taken at 50 mV s^{-1}) of (a) Ir and (b) Co before (blue) and after (black) durability.

was accompanied by higher dissolution rates (>5%). The Ir dissolution rate, however, was less than in acid and may be reflective of faster oxide growth in base and the effect of oxides slowing dissolution kinetics.[14] Following a 2 V hold, however, Ir cyclic voltammograms showed thinning (not limited to hydrogen underpotential deposition), indicating that less catalyst was present and that dissolution or Ir loss was a significant contributor to lower performance (Fig. 6).

For Co, losses occurred at moderate and high potential. For the potentials evaluated, Co surfaces were expected to oxidize/passivate (oxidation to $Co(OH)_3$). In Co durability experiments and regardless of potential, low dissolution rates were found (<4%, Fig. 5a) along with comparatively small changes to the cyclic voltammograms in the double charging layer and Co redox. In terms of dissolution, a maximum of 3.5% was found following a 2.2 V hold; the dissolution rate, however, dropped at higher potential (2.5 V) and dissolution/oxidation of the Au substrate may have impacted testing. Following extended operation at elevated potential, the Co specific activity dropped and approached that of Co oxide (Co_3O_4, initial activity). These results suggest that oxide growth, not dissolution, was the primary source of performance loss.

Single-cell catalyst performance.—In MEA testing, performance was evaluated with full polarization curves and Tafel plots that focused on kinetic performance (Fig. 7). The PGM catalysts (Ir, Ir oxide) generally outperformed the non-PGM catalysts (Co, Co oxide), expected from the RDE results. In the kinetic region (1.5 V), the Ir MEA produced 1370 A g_{Ir}^{-1} compared to 101 A g_{Co}^{-1} for the Co MEA. This activity gap (14.2 times) is smaller than observed in RDE (26.2 times), and various factors impact MEA performances, including: catalyst loading, where Co required a higher loading due to the larger particle size; catalyst layer integration (ionomer, membrane); and test conditions that may modify catalyst surfaces and structures. The metal oxides were also slightly lower performing in MEAs than their metal counterparts. The difference between Co/Co_3O_4 and Ir/IrO_2 performance, however, was much smaller than in RDE testing and

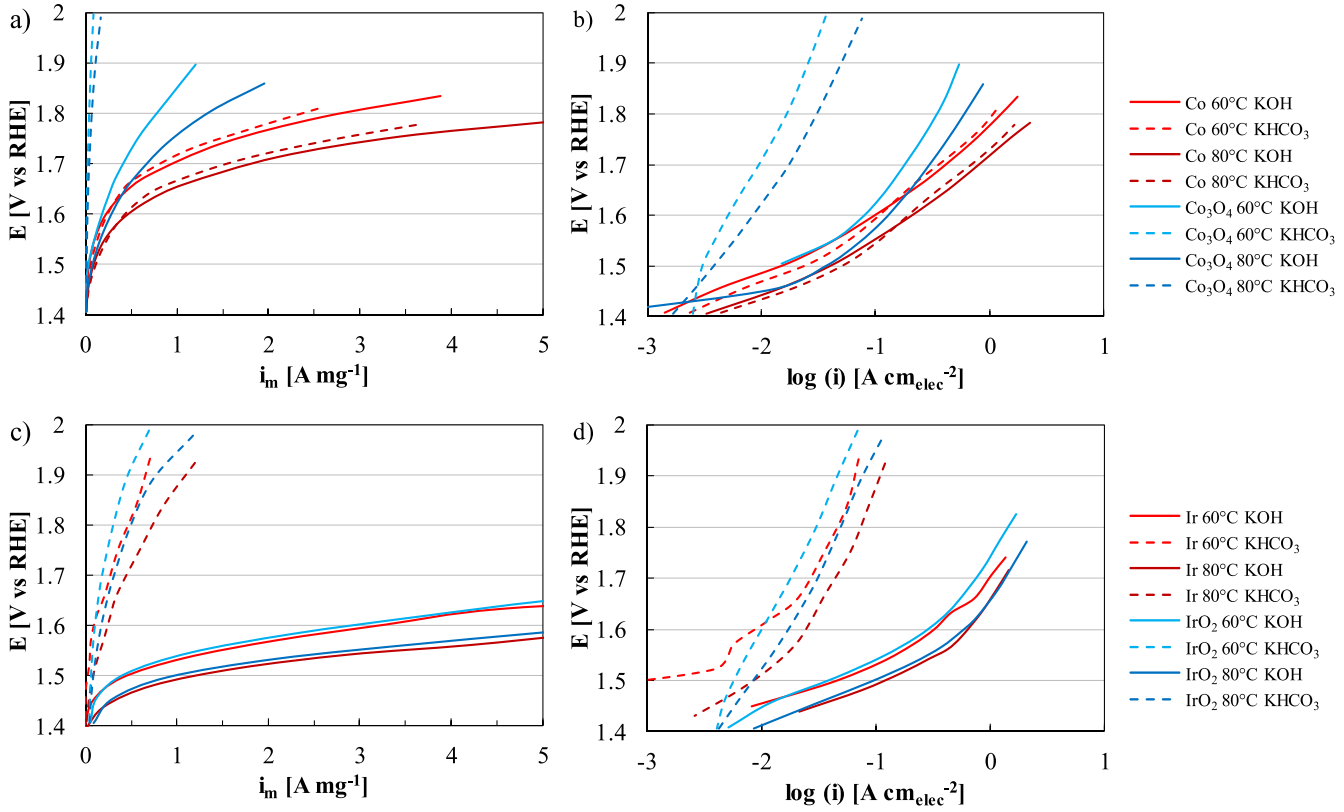

Figure 7. Single cell polarization curves of (a), (b) Co and Co_3O_4, and (c), (d) Ir and IrO_2 anodes (Pt/HSC cathodes) in 1 M KOH (solid) and 0.1 M potassium bicarbonate ($KHCO_3$, dashed) at 60 °C (red) and 80 °C (blue). Data was presented at in terms of (a), (c) full polarization curves and (b), (d) Tafel plots.

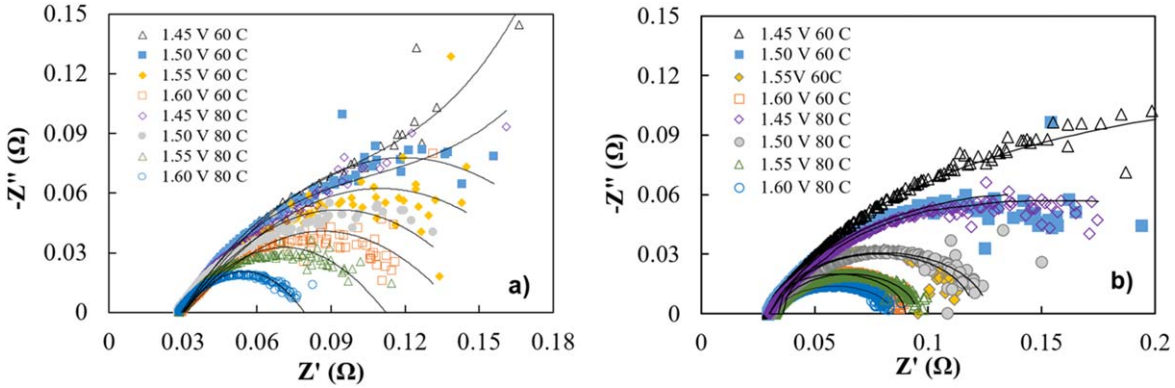

Figure 8. Electrochemical impedance spectroscopy for (a) Co and (b) IrO_2 anodes (Pt/HSC cathodes) in single cell electrolyzer tests in 1 M KOH at 60 °C and 80 °C.

likely due to surface oxidation inhibiting catalyst activity. While oxide growth is typically minimized in RDE tests, MEA testing can exacerbate oxide growth due to the elevated temperature (60 °C, 80 °C), higher potential (conditioning at 2 V), and longer operation time (4 h) of single-cell conditioning.[14] Oxide growth in MEAs may also account for differences between RDE/MEA performance. While the Ir/Co performance gap was smaller in MEAs (14.2 times) than RDEs (26.2 times), the RDE results were comparable if the catalysts were held at elevated potential (1.6 V hold for 13.5 h, 16.9 times). These results suggest that some degree of oxide growth in RDEs may be necessary to project kinetic performance at the device level, and that extended operation or conditioning in RDEs may be needed to assess catalyst improvements. MEAs were also tested in potassium bicarbonate to assess the effect on performance. For most of the catalysts tested, the performance in $KHCO_3$ was lower than in KOH. For Co, however, the MEA performance in the kinetic region was greater in $KHCO_3$, although the transport losses were slightly higher.

Electrochemical impedance spectroscopy was also conducted for Co and IrO_2 anodes (Pt/HSC cathodes) in a single cell. Both MEAs had similar high frequency resistances (0.03 Ω), expected since both tests used the same membrane and hardware (flow fields, Fig. 8). Similar HFR values further suggested that the anode catalysts produced minimal and comparable contact resistances that did not adversely affect cell performance. At higher current density, the impedance spectra generally fit a Randles cell, indicating that kinetics had a larger impact than transport on MEA performance.[122]

Several differences were noted between RDE and MEA testing. Ohmic losses were larger in RDE and a function of the distance between electrodes (22–25 Ω); the membranes used, however, were relatively thin and the ohmic losses less than in typical PEM systems.[123] Transport losses were also larger in RDEs, and differences in testing including the electrode alignment and electrolyte flow (convection in RDE, forced flow in MEA) affected the onset of transport. Transport losses in AEM MEAs, however, tended to be larger than in PEM when using the same transport layers and similar hardware (flow fields) and may be impacted by spraying the catalyst onto the transport layers (as opposed to the membrane). Kinetics were generally faster in MEAs when using a supporting alkaline electrolyte, particularly when accounting for oxide growth. While RDE/MEA mass activities were 1–2 orders of magnitude apart for metal nanoparticles, including Ir (1370 A g_{Ir}^{-1} in MEA, 68 A g_{Ir}^{-1} in RDE at 1.5 V) and Co (101 A g_{Co}^{-1} in MEA, 0.75 A g_{Co}^{-1} in RDE at 1.5 V), the gap was an order of magnitude larger for materials that were oxides ex situ. This difference is similar to one previously found in PEM electrolyzers (RDE with acidic electrolytes) and may be due to differences in temperature and interface (membrane/ionomer, RDE electrolyte).[14]

Conclusions

RDE testing is used to screen catalysts to project kinetic improvements at the device level. Due to the wide range of baseline catalyst activities reported in literature, however, standardizing test procedures and benchmarking standard materials is critical.

Several commercial non-PGM and PGM catalysts were tested for OER activity to establish baseline activity. Catalysts that started as metals ex situ tended to be more active than their oxidized counter parts. This trend was exaggerated in RDE tests due to the short break-in procedures which can mitigate near-surface oxide formation. In single-cell testing, oxide formation was unavoidable and metal catalyst performances were lower and approached that of oxides, decreasing the gap between metal and metal-oxide performance found in RDE. Co nanoparticles had the largest OER activity and the smallest overpotential of the non-PGMs (1.48 V in RDE) and produced promising performance in AEM electrolyzers (12 A g^{-1} at 1.55 V). While Ru catalysts had small overpotentials (1.38 V in RDE), they dissolved quickly at elevated potential and Ir was therefore used as the PGM baseline. RDE durability tests were completed on Co and Ir. At higher potentials, Ir had higher catalyst losses and higher levels of dissolution which peaked at 15% (cycling between 1.4 V to 2.0 V). For Co, however, smaller amounts of dissolution were found and Co along with other non-PGM catalysts are promising due to the tendency to oxidize but not dissolve. While significant dissolution did not occur, loss due to oxide growth did, and some exposure to elevated potential may be necessary to project kinetic improvements at the device level.

Capital or catalyst cost is not a primary driver in commercial electrolysis today. To become cost competitive, however, electrolyzers need to shift from retail electricity to load following low cost, renewable power sources. At that point, addressing the higher capital and catalyst cost at lower capacity is necessary, and understanding and improving catalyst performance and durability is critical. Establishing baseline catalyst performance is vital to comparing the performance of newly developed catalysts and projecting device-level improvements. A significant need remains for developing durable and highly active catalysts to become enabling elements in AEM-based electrolyzers. Further implementation of half-cell baselines is needed to reasonably project device level performance and to direct catalyst development efforts.

Acknowledgments

This work was authored by the National Renewable Energy Laboratory, operated by Alliance for Sustainable Energy, LLC, for the U.S. Department of Energy (DOE) under Contract No. DE-AC36–08GO28308. Funding provided by U.S. Department of Energy Office of Energy Efficiency and Renewable Energy Fuel Cell Technologies Office. The views expressed in the article do not necessarily represent the views of the DOE or the U.S. Government. The U.S. Government retains and the publisher, by accepting the article for publication, acknowledges that the U.S. Government retains a nonexclusive, paid-up, irrevocable, worldwide license to

References

1. A. Ursua, L. M. Gandia, and P. Sanchis, *Proc. of the IEEE*, **100**, 410 (2011).
2. B. Pivovar, N. Rustagi, and S. Satyapal, *Electrochem. Soc. Interface*, **27**, 47 (2018).
3. C. C. McCrory, S. Jung, J. C. Peters, and T. F. Jaramillo, *JACS*, **135**, 16977 (2013).
4. S. M. Alia and G. C. Anderson, *J. Electrochem. Soc.*, **166**, F282 (2019).
5. S. M. Alia and B. S. Pivovar, *J. Electrochem. Soc.*, **165**, F441 (2018).
6. K. Shinozaki, J. W. Zack, R. M. Richards, B. S. Pivovar, and S. S. Kocha, *J. Electrochem. Soc.*, **162**, F1144 (2015).
7. D. A. Corrigan, *J. Electrochem. Soc.*, **134**, 377 (1987).
8. L. Trotochaud, S. L. Young, J. K. Ranney, and S. W. Boettcher, *JACS*, **136**, 6744 (2014).
9. S. M. Alia, B. Rasimick, C. Ngo, K. C. Neyerlin, S. S. Kocha, S. Pylypenko, H. Xu, and B. S. Pivovar, *J. Electrochem. Soc.*, **163**, F3105 (2016).
10. R. Woods, *J. Electroanal. Chem. Interfacial Electrochem.*, **49**, 217 (1974).
11. S. M. Alia, K. E. Hurst, S. S. Kocha, and B. S. Pivovar, *J. Electrochem. Soc.*, **163**, F3051 (2016).
12. Z. Liu, S. D. Sajjad, Y. Gao, J. Kaczur, and R. Masel, *ECS Trans.*, **77**, 71 (2017).
13. I. C. Man, H. Y. Su, F. Calle-Vallejo, H. A. Hansen, J. I. Martínez, N. G. Inoglu, J. Kitchin, T. F. Jaramillo, J. K. Nørskov, and J. Rossmeisl, *Chem. Cat. Chem.*, **3**, 1159 (2011).
14. S. M. Alia, M.-A. Ha, G. C. Anderson, C. Ngo, S. Pylypenko, and R. E. Larsen, *J. Electrochem. Soc.*, **166**, F1243 (2019).
15. L. Ai, Z. Niu, and J. Jiang, *Electrochim. Acta*, **242**, 355 (2017).
16. M.-S. Balogun, W. Qiu, H. Yang, W. Fan, Y. Huang, P. Fang, G. Li, H. Ji, and Y. Tong, *Energy Environ. Sci.*, **9**, 3411 (2016).
17. G. F. Chen, T. Y. Ma, Z. Q. Liu, N. Li, Y. Z. Su, K. Davey, and S. Z. Qiao, *Adv. Funct. Mater.*, **26**, 3314 (2016).
18. Y. Cheng, C. Xu, L. Jia, J. D. Gale, L. Zhang, C. Liu, P. K. Shen, and S. P. Jiang, *Appl. Catal. B*, **163**, 96 (2015).
19. B. Cui, H. Lin, J. B. Li, X. Li, J. Yang, and J. Tao, *Adv. Funct. Mater.*, **18**, 1440 (2008).
20. L.-L. Feng, G. Yu, Y. Wu, G.-D. Li, H. Li, Y. Sun, T. Asefa, W. Chen, and X. Zou, *JACS*, **137**, 14023 (2015).
21. P. Ganesan, A. Sivanantham, and S. Shanmugam, *J. Mater. Chem. A*, **4**, 16394 (2016).
22. H. Jin, J. Wang, D. Su, Z. Wei, Z. Pang, and Y. Wang, *JACS*, **137**, 2688 (2015).
23. M. Ledendecker, S. Krick Calderón, C. Papp, H. P. Steinrück, M. Antonietti, and M. Shalom, *Angew. Chem.*, **127**, 12538 (2015).
24. Y. Li, H. Zhang, M. Jiang, Y. Kuang, X. Sun, and X. Duan, *Nano Res.*, **9**, 2251 (2016).
25. Z.-Y. Li, S.-T. Shi, Q.-S. Zhong, C.-J. Zhang, and C.-W. Xu, *Electrochim. Acta*, **146**, 119 (2014).
26. Y. Liang, Q. Liu, Y. Luo, X. Sun, Y. He, and A. M. Asiri, *Electrochim. Acta*, **190**, 360 (2016).
27. Y. Libin, Q. Honglan, Z. Chengxiao, and S. Xuping, *Nanotechnology*, **27**, 23LT01 (2016).
28. Q. Liu, S. Gu, and C. M. Li, *J. Power Sources*, **299**, 342 (2015).
29. T. Liu, X. Sun, A. M. Asiri, and Y. He, *Int. J. Hydrogen Energy*, **41**, 7264 (2016).
30. W. Lu et al., *Small*, **13**, 1700805 (2017).
31. Y. Meng, W. Song, H. Huang, Z. Ren, S.-Y. Chen, and S. L. Suib, *JACS*, **136**, 11452 (2014).
32. M. H. Miles, *J. Electroanal. Chem. Interfacial Electrochem.*, **60**, 89 (1975).
33. C. Ouyang, X. Wang, C. Wang, X. Zhang, J. Wu, Z. Ma, S. Dou, and S. Wang, *Electrochim. Acta*, **174**, 297 (2015).
34. Y. Pi, N. Zhang, S. Guo, J. Guo, and X. Huang, *Nano Lett.*, **16**, 4424 (2016).
35. M. Shalom, D. Ressnig, X. Yang, G. Clavel, T. P. Fellinger, and M. Antonietti, *J. Mater. Chem. A*, **3**, 8171 (2015).
36. J. Shi, J. Hu, Y. Luo, X. Sun, and A. M. Asiri, *Catal. Sci. Technol.*, **5**, 4954 (2015).
37. Y. Tan, C. Wu, H. Lin, J. Li, B. Chi, J. Pu, and L. Jian, *Electrochim. Acta*, **121**, 183 (2014).
38. C. Tang, A. M. Asiri, Y. Luo, and X. Sun, *Chem. Nano. Mat*, **1**, 558 (2015).
39. J. Tian, N. Cheng, Q. Liu, X. Sun, Y. He, and A. M. Asiri, *J. Mater. Chem. A*, **3**, 20056 (2015).
40. Y. Wang, C. Xie, D. Liu, X. Huang, J. Huo, and S. Wang, *ACS Appl. Mater. Interfaces*, **8**, 18652 (2016).
41. C. Xia, Q. Jiang, C. Zhao, M. N. Hedhili, and H. N. Alshareef, *Adv. Mater.*, **28**, 77 (2015).
42. L. Yanhui, S. Xuping, M. A. Abdullah, and H. Yuquan, *Nanotechnology*, **27**, 12LT01 (2016).
43. Y. Zhao, R. Nakamura, K. Kamiya, S. Nakanishi, and K. Hashimoto, *Nat. Commun.*, **4**, 2390 (2013).
44. W. Zhu, X. Yue, W. Zhang, S. Yu, Y. Zhang, J. Wang, and J. Wang, *Chem. Commun.*, **52**, 1486 (2016).
45. W. Fang, D. Liu, Q. Lu, X. Sun, and A. M. Asiri, *Electrochem. Commun.*, **63**, 60 (2016).
46. J. Wang, W. Yang, and J. Liu, *J. Mater. Chem. A*, **4**, 4686 (2016).
47. P. Chen, K. Xu, T. Zhou, Y. Tong, J. Wu, H. Cheng, X. Lu, H. Ding, C. Wu, and Y. Xie, *Angew. Chem. Int. Ed.*, **55**, 2488 (2016).
48. J. B. Gerken, J. G. McAlpin, J. Y. C. Chen, M. L. Rigsby, W. H. Casey, R. D. Britt, and S. S. Stahl, *JACS*, **133**, 14431 (2011).
49. Y. Jia et al., *Adv. Mater.*, **29**, 1700017 (2017).
50. J. Jiang, A. Zhang, L. Li, and L. Ai, *J. Power Sources*, **278**, 445 (2015).
51. N. Jiang, B. You, M. Sheng, and Y. Sun, *Angew. Chem.*, **127**, 6349 (2015).
52. L. Jiao, Y.-X. Zhou, and H.-L. Jiang, *Chem. Sci.*, **7**, 1690 (2016).
53. Z. Jin, P. Li, and D. Xiao, *Green Chem.*, **18**, 1459 (2016).
54. A. Grimaud, A. Demortière, M. Saubanère, W. Dachraoui, M. Duchamp, M.-L. Doublet, and J.-M. Tarascon, *Nat. Energy*, **2**, 16189 (2016).
55. S. Li, Y. Wang, S. Peng, L. Zhang, A. M. Al-Enizi, H. Zhang, X. Sun, and G. Zheng, *Adv. Energy Mater.*, **6**, 1501661 (2016).
56. S. Xu, Y. Liu, J. Tong, W. Hu, and Q. Xia, *Russ. J. Electrochem.*, **52**, 1021 (2016).
57. L. Liu, Y. Ou, D. Gao, L. Yang, H. Dong, P. Xiao, and Y. Zhang, *J. Power Sources*, **396**, 395 (2018).
58. X. Lu and C. Zhao, *J. Mater. Chem. A*, **1**, 12053 (2013).
59. L.-A. Stern, L. Feng, F. Song, and X. Hu, *Energy Environ. Sci.*, **8**, 2347 (2015).
60. T. Takashima, K. Hashimoto, and R. Nakamura, *JACS*, **134**, 1519 (2012).
61. P. Lettenmeier, J. Majchel, L. Wang, A. S. Gago, and K. A. Friedrich, *ECS Trans.*, **72**, 1 (2016).
62. J. Wu, Y. Xue, X. Yan, W. Yan, Q. Cheng, and Y. Xie, *Nano Res.*, **5**, 521 (2012).
63. X. Xu, P. Du, Z. Chen, and M. Huang, *J. Mater. Chem. A*, **4**, 10933 (2016).
64. Y. Yan, B. Y. Xia, X. Ge, Z. Liu, A. Fisher, and X. Wang, *Chem.—Eur. J.*, **21**, 18062 (2015).
65. Y. Zhan, G. Du, S. Yang, C. Xu, M. Lu, Z. Liu, and J. Y. Lee, *ACS Appl. Mater. Interfaces*, **7**, 12930 (2015).
66. X. Zhang, S. Liu, Y. Zang, R. Liu, G. Liu, G. Wang, Y. Zhang, H. Zhang, and H. Zhao, *Nano Energy*, **30**, 93 (2016).
67. W. Zhou, M. Zhao, F. Liang, S. C. Smith, and Z. Zhu, *Mater. Horiz.*, **2**, 495 (2015).
68. D. Li, H. Baydoun, C. u. N. Verani, and S. L. Brock, *JACS*, **138**, 4006 (2016).
69. X. Li, Z. Niu, J. Jiang, and L. Ai, *J. Mater. Chem. A*, **4**, 3204 (2016).
70. X. Lu and C. Zhao, *Nat. Commun.*, **6**, 6616 (2015).
71. C. Wang, J. Jiang, T. Ding, G. Chen, W. Xu, and Q. Yang, *Adv. Mater. Interfaces*, **3**, 1500454 (2016).
72. Y. Zhao, S. Chen, B. Sun, D. Su, X. Huang, H. Liu, Y. Yan, K. Sun, and G. Wang, *Sci. Rep.*, **5**, 7629 (2015).
73. J. Chang, Y. Xiao, M. Xiao, J. Ge, C. Liu, and W. Xing, *ACS Catal.*, **5**, 6874 (2015).
74. J. Y. C. Chen, L. Dang, H. Liang, W. Bi, J. B. Gerken, S. Jin, E. E. Alp, and S. S. Stahl, *JACS*, **137**, 15090 (2015).
75. G. Gardner, J. Al-Sharab, N. Danilovic, Y. B. Go, K. Ayers, M. Greenblatt, and G. Charles Dismukes, *Energy Environ. Sci.*, **9**, 184 (2016).
76. G. Kreysa and B. Håkansson, *J. Electroanal. Chem. Interfacial Electrochem.*, **201**, 61 (1986).
77. M. Liao, G. Zeng, T. Luo, Z. Jin, Y. Wang, X. Kou, and D. Xiao, *Electrochim. Acta*, **194**, 59 (2016).
78. X. Liu, X. Wang, X. Yuan, W. Dong, and F. Huang, *J. Mater. Chem. A*, **4**, 167 (2016).
79. Y. Qiu, L. Xin, and W. Li, *Langmuir*, **30**, 7893 (2014).
80. R. N. Singh, D. Mishra, Anindita, A. S. K. Sinha, and A. Singh, *Electrochem. Commun.*, **9**, 1369 (2007).
81. G. Wu, N. Li, D.-R. Zhou, K. Mitsuo, and B.-Q. Xu, *J. Solid State Chem.*, **177**, 3682 (2004).
82. Y. Yang, H. Fei, G. Ruan, C. Xiang, and J. M. Tour, *ACS Nano*, **8**, 9518 (2014).
83. M. P. Browne, H. Nolan, G. S. Duesberg, P. E. Colavita, and M. E. G. Lyons, *ACS Catal.*, **6**, 2408 (2016).
84. D. Chanda, J. Hnát, M. Paidar, and K. Bouzek, *Int. J. Hydrogen Energy*, **39**, 5713 (2014).
85. S. Chen, J. Duan, M. Jaroniec, and S. Z. Qiao, *Angew. Chem. Int. Ed.*, **52**, 13567 (2013).
86. H. Dumont, P. Los, L. Brossard, A. Lasia, and H. Ménard, *J. Electrochem. Soc.*, **139**, 2143 (1992).
87. M. S. El-Deab, M. I. Awad, A. M. Mohammad, and T. Ohsaka, *Electrochem. Commun.*, **9**, 2082 (2007).
88. Y.-J. Huang, C.-H. Lai, P.-W. Wu, and L.-Y. Chen, *J. Electrochem. Soc.*, **157**, P18 (2010).
89. A. N. Jain, S. K. Tiwari, R. N. Singh, and P. Chartier, *J. Chem. Soc., Faraday Trans.*, **91**, 1871 (1995).
90. C. Kjartansdóttir, M. Caspersen, S. Egelund, and P. Møller, *Electrochim. Acta*, **142**, 324 (2014).
91. Y. Li, P. Hasin, and Y. Wu, *Adv. Mater.*, **22**, 1926 (2010).
92. T. Malinski, A. Ciszewski, J. Bennett, J. R. Fish, and L. Czuchajowski, *J. Electrochem. Soc.*, **138**, 2008 (1991).
93. E. Rios, P. Chartier, and J. L. Gautier, *Solid State Sci.*, **1**, 267 (1999).
94. R. N. Singh, S. K. Tiwari, S. P. Singh, N. K. Singh, G. Poillerat, and P. Chartier, *J. Chem. Soc., Faraday Trans.*, **92**, 2593 (1996).
95. A. Wattiaux, J. C. Grenier, M. Pouchard, and P. Hagenmuller, *J. Electrochem. Soc.*, **134**, 1714 (1987).
96. X. Wu and K. Scott, *J. Mater. Chem.*, **21**, 12344 (2011).
97. X. Zhang, R. Liu, Y. Zang, G. Liu, G. Wang, Y. Zhang, H. Zhang, and H. Zhao, *Chem. Commun.*, **52**, 5946 (2016).
98. Y. Lee, J. Suntivich, K. J. May, E. E. Perry, and Y. Shao-Horn, *J. Phys. Chem. Letters*, **3**, 399 (2012).
99. F. Liang, Y. Yu, W. Zhou, X. Xu, and Z. Zhu, *J. Mater. Chem. A*, **3**, 634 (2015).
100. M.-R. Gao, X. Cao, Q. Gao, Y.-F. Xu, Y.-R. Zheng, J. Jiang, and S.-H. Yu, *ACS Nano*, **8**, 3970 (2014).

101. Y. Gorlin and T. F. Jaramillo, *JACS*, **132**, 13612 (2010).
102. M. Gong, Y. Li, H. Wang, Y. Liang, J. Z. Wu, J. Zhou, J. Wang, T. Regier, F. Wei, and H. Dai, *JACS*, **135**, 8452 (2013).
103. H. Wang, H.-W. Lee, Y. Deng, Z. Lu, P.-C. Hsu, Y. Liu, D. Lin, and Y. Cui, *Nat. Commun.*, **6**, 7261 (2015).
104. Y. Zhu, W. Zhou, Z. G. Chen, Y. Chen, C. Su, M. O. Tadé, and Z. Shao, *Angew. Chem. Int. Ed.*, **54**, 3897 (2015).
105. Y. Zhu, W. Zhou, Y. Zhong, Y. Bu, X. Chen, Q. Zhong, M. Liu, and Z. Shao, *Adv. Energy Mater.*, **7** (2016).
106. T. Maiyalagan, K. A. Jarvis, S. Therese, P. J. Ferreira, and A. Manthiram, *Nat. Commun.*, **5**, 3949 (2014).
107. J. Parrondo, M. George, C. Capuano, K. E. Ayers, and V. Ramani, *J. Mater. Chem. A*, **3**, 10819 (2015).
108. Y. Yang, H. Fei, G. Ruan, and J. M. Tour, *Adv. Mater.*, **27**, 3175 (2015).
109. B. Zhang, C. Xiao, S. Xie, J. Liang, X. Chen, and Y. Tang, *Chem. Mater.*, **28**, 6934 (2016).
110. Y. Wu, G. D. Li, Y. Liu, L. Yang, X. Lian, T. Asefa, and X. Zou, *Adv. Funct. Mater.*, **26**, 4839 (2016).
111. T. Liu, A. M. Asiri, and X. Sun, *Nanoscale*, **8**, 3911 (2016).
112. T. Liu, Q. Liu, A. M. Asiri, Y. Luo, and X. Sun, *Chem. Commun.*, **51**, 16683 (2015).
113. B. You and Y. Sun, *Adv. Energy Mater.*, **6**, 1502333 (2016).
114. L. Trotochaud, J. K. Ranney, K. N. Williams, and S. W. Boettcher, *JACS*, **134**, 17253 (2012).
115. J. Wang, D. Gao, G. Wang, S. Miao, H. Wu, J. Li, and X. Bao, *J. Mater. Chem. A*, **2**, 20067 (2014).
116. X. Cui, P. Ren, D. Deng, J. Deng, and X. Bao, *Energy Environ.Sci.*, **9**, 123 (2016).
117. F. Song and X. Hu, *JACS*, **136**, 16481 (2014).
118. J. A. Vigil, T. N. Lambert, and B. T. Christensen, *J. Mater. Chem. A*, **4**, 7549 (2016).
119. X. Liu, Z. Chang, L. Luo, T. Xu, X. Lei, J. Liu, and X. Sun, *Chem. Mater.*, **26**, 1889 (2014).
120. Y. Jin, H. Wang, J. Li, X. Yue, Y. Han, P. K. Shen, and Y. Cui, *Adv. Mater.*, **28**, 3785 (2016).
121. M. Pourbaix, in *Atlas of Electrochemical Equilibria in Aqueous Solution* (National Association of Corrosion Engineers, Houston, TX) (1974).
122. F. Mansfeld, "Analysis and interpretation of EIS data for metals and alloys." *Technical Report*, Solartron Analytical (1993).
123. S. M. Alia, S. Stariha, and R. L. Borup, *J. Electrochem. Soc.*, **166**, F1164 (2019).